Chlorotoxin Labeled Magnetic Nanovectors for Targeted Gene Delivery to Glioma

Forrest M. Kievit,[†] Omid Veiseh,[†] Chen Fang,[†] Narayan Bhattarai,[†] Donghoon Lee,[‡] Richard G. Ellenbogen,[§] and Miqin Zhang*,[†,‡,§]

[†]Department of Materials Science and Engineering, [‡]Department of Radiology, and [§]Department of Neurological Surgery, University of Washington, Seattle, Washington 98195

Gene therapy has the potential to effectively medicate cancer by treating the root of the disease: DNA damage that results in aberrant cell signaling leading to uncontrolled cell growth and tumor formation. This technology involves the delivery of DNA molecules to cancer cells to insert or modify a gene in an effort to treat the disease. The delivery of DNA can be accomplished using a variety of vectors, including viruses, cell-based systems, and synthetic vectors. For glioma gene therapy, viral vectors have been used to deliver suicide genes, pro-apoptotic genes, p53, cytokines, and caspases.[1] These studies have shown promising preclinical results, but clinical trials have been limited by the fact that transduced cells were found only within a very short distance of the delivery site. Furthermore, concerns over safety and potential side effects have slowed their advancement into the clinic.[2,3] To overcome these limitations, synthetic vectors, such as cationic polymers, peptides, liposomes, and solid-core nanoparticles, have been developed to more safely deliver DNA. These systems have shown promise *in vitro* but exhibit significantly reduced transfection efficiencies *in vivo* due to lack of site specificity and limited internalization by cancer cells.[4]

Many synthetic gene delivery vehicles rely on the enhanced permeability and retention (EPR) effect to passively accumulate in the tumor site for access to cancer cells. One strategy to improve the accumulation of gene delivery vehicles in the tumor site is magnetofection, where magnetic nanoparticle-based gene delivery vehicles are magnetically driven into the tumor site.[5,6] While this strategy works well for solid tumor masses, it provides little advantage for highly invasive and infiltrative cancers, such as glioma, the most common and lethal type of brain cancers,[7−9] since these cells would not be accessible by a magnet. Another strategy to improve the gene delivery vehicle uptake by cancer cells is through the attachment of targeting ligands. The attachment of tumor-targeting antibodies, peptides, and small molecules onto the surface of gene delivery vehicles has been shown to enhance the uptake of these vehicles by cancer cells *in vivo* through receptor-mediated endocytosis and to provide higher transfection efficiencies.[10−17]

For glioma, a number of targeting molecules have been evaluated, including chlorotoxin (CTX),[18] epidermal growth factor receptor (EGFR) antibodies,[19] transferrin,[20] F3 homing peptide,[21,22] insulin receptor antibodies,[23] cationic albumin,[24] and methotrexate.[25] Among these identified targeting

ABSTRACT Glioma accounts for 80% of brain tumors and currently remains one of the most lethal forms of cancers. Gene therapy could potentially improve the dismal prognosis of patients with glioma, but this treatment modality has not yet reached the bedside from the laboratory due to the lack of safe and effective gene delivery vehicles. In this study we investigate targeted gene delivery to C6 glioma cells in a xenograft mouse model using chlorotoxin (CTX) labeled nanoparticles. The developed nanovector consists of an iron oxide nanoparticle core, coated with a copolymer of chitosan, polyethylene glycol (PEG), and polyethylenimine (PEI). Green fluorescent protein (GFP) encoding DNA was bound to these nanoparticles, and CTX was then attached using a short PEG linker. Nanoparticles without CTX were also prepared as a control. Mice bearing C6 xenograft tumors were injected intravenously with the DNA-bound nanoparticles. Nanoparticle accumulation in the tumor site was monitored using magnetic resonance imaging and analyzed by histology, and GFP gene expression was monitored through Xenogen IVIS fluorescence imaging and confocal fluorescence microscopy. Interestingly, the CTX did not affect the accumulation of nanoparticles at the tumor site but specifically enhanced their uptake into cancer cells as evidenced by higher gene expression. These results indicate that this targeted gene delivery system may potentially improve treatment outcome of gene therapy for glioma and other deadly cancers.

KEYWORDS: Gene delivery · cancer · chlorotoxin · targeting · nanoparticle · iron oxide · chitosan
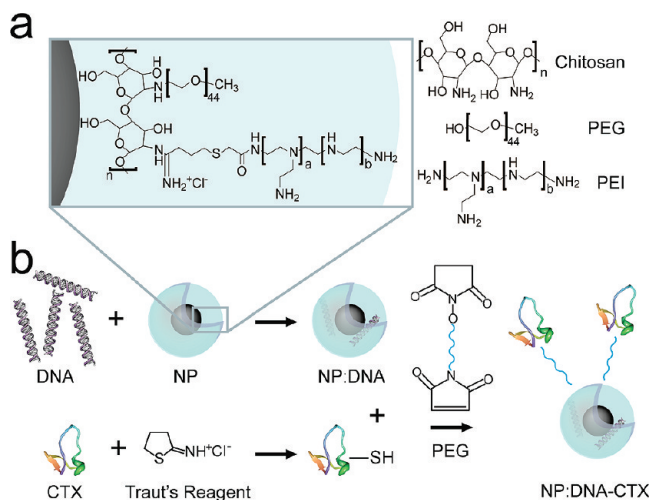
Figure 1. Schematic of NP:DNA−CTX nanovector synthesis. (a) The iron oxide nanoparticle core was coated with a copolymer of chitosan, PEG, and PEI to produce NP. (b) DNA was loaded into NP through the electrostatic interaction between negatively charged DNA and positively charged NP coating to form NP:DNA. The reactive amine groups of chlorotoxin (CTX) were modified with Traut's reagent to render a free thiol group. CTX was conjugated onto NP:DNA to form NP:DNA−CTX through a heterobifunctional PEG linker (NHS-PEG−maleimide) to ensure CTX was free to interact with target cells.

ligands, CTX has emerged as a promising targeting agent due to its ability to specifically recognize a broad spectrum of cancers, including the vast majority of brain tumors, prostate, skin, and colorectal cancers.[26−31] CTX is internalized by glioma cells and has been shown to be trafficked to the perinuclear region when attached to iron oxide nanoparticles,[30] making it an ideal targeting agent for gene delivery. Furthermore, the attachment of CTX to iron oxide nanoparticles coated with chitosan and polyethylene glycol (PEG) enables them to bypass the blood−brain barrier,[18] which provides an optimal platform for the further development of this nanoparticle system as a gene delivery nanovector for glioma.

We previously developed a nonviral gene delivery nanovector that comprises an iron oxide nanoparticle core coated with a copolymer of chitosan, PEG, and polyethylenimine (PEI).[32] The iron oxide core is desirable due to its superparamagnetic property that provides contrast in magnetic resonance imaging (MRI) allowing for noninvasive, *in situ* monitoring of nanovector accumulation. Chitosan is a cationic, biocompatible polymer derived from the exoskeletons of crustaceans and, along with PEG, provides a highly stable coating for nanoparticles enabling excellent biodistribution and blood half-life.[18,33] PEI was included in the polymer coating to provide an improved DNA binding efficiency and a mechanism to escape the endosome through the proton sponge effect.[12,32,34] This nanovector (NP) was able to effectively bind DNA (NP:DNA), protect it from degradation, and successfully deliver it to the tumor site for expression by cancer cells.[32]

In this study, we aimed to enhance gene delivery specifically to glioma cells by incorporating the targeting ligand, CTX, onto the surface of the nanovector to elicit glioma cell-specific, receptor-mediated endocytosis. DNA encoding green fluorescent protein (GFP) was used for optical monitoring of gene expression. Mice bearing C6 rat glioma xenograft flank tumors, a highly malignant and invasive model of glioma,[35] were treated with DNA-loaded, CTX-activated nanovectors. Nanovector accumulation in the tumor site was monitored using MRI and analyzed by histology, and nanovector uptake into cells was monitored through gene expression using Xenogen and confocal fluorescence imaging.

RESULTS AND DISCUSSION

Nanovector Development. Iron oxide nanoparticles coated with a copolymer of chitosan, PEG, and PEI were prepared, as previously described,[32] and herein called NP (Figure 1a). Figure 1b shows the schematic for loading DNA into the coating on NP and the functionalization of NP with CTX. As illustrated, DNA was encapsulated into NP through the electrostatic interaction between the negatively charged DNA and the positively charged polymer coating to form NP:DNA. CTX was first thiolated through reaction with 2-iminothiolane (Traut's reagent) in preparation for attachment to the NP:DNA surface. A heterobifunctional PEG linker, NHS-PEG$_{12}$−maleimide, was conjugated to amine functional groups available on the polymer coating (from PEI and chitosan) on NP. Subsequently the thiolated CTX was reacted with the maleimide reactive portion of the PEG linker, anchoring CTX to the surface of the DNA-bound NP to form NP:DNA−CTX.

Energy dispersive X-ray (EDX) spectrometry analysis of NP:DNA showed peaks of iron (Fe) from the iron oxide nanoparticle core, carbon (C), nitrogen (N), sulfur (S), and oxygen (O) which confirmed the presence of the polymer coating and phosphorus (P) which confirmed the presence of DNA (Figure 2a). Peaks associated with copper (Cu), magnesium (Mg), and silicon (Si) were from the transmission electron microscopy (TEM) grid. The size of the iron oxide core was 7.5 nm, as determined previously.[18]

The hydrodynamic size, which is a measure of the NP core plus polymer coating and bound DNA, is a physiologically relevant measure since this is the effective size of the NP that will be seen by cells in the body. NPs larger than 100 nm will be easily taken up by macrophage cells of the reticulo-endothelial system (RES), while NPs smaller than 10 nm will be filtered out by the kidneys.[36,37] To minimize potential elimination of nanovectors from the body, the developed nanovector should be between 10 and 100 nm. NP:DNA and NP:DNA−CTX were analyzed using dynamic light scattering and found to have hydrodynamic diameters of 43.5 and 48.8 nm, respectively (Figure 2b), which are well within the desired size range. The minimal size differ-

ence between NP:DNA and NP:DNA−CTX ensures that any differences seen in tissue accumulation and nanovector uptake by cells are due primarily to the presence of the targeting agent (CTX) but not to the differences in clearance or EPR effect.[38] Furthermore, the size range exhibited by our nanovectors (~40 nm) is favorable for NP uptake by cancer cells.[39]

The ζ potential, or surface charge on the NP, is another important parameter that would affect the transfection efficiency of a gene delivery nanovector. For NP: DNA and NP:DNA−CTX specifically, a positive ζ potential suggests that DNA is fully encapsulated into the polymer coating.[32] Both NP:DNA and NP:DNA−CTX had positive ζ potentials of 15.2 and 17.7 mV, respectively, and a similar narrow distribution (Figure 2c). As with the NP sizes, similar ζ potentials will also ensure that differences seen in NP accumulation in tissues and uptake by target cells are primarily due to the presence or absence of CTX. The number of CTX molecules per nanoparticle was estimated to be 5 for NP: DNA−CTX, and the number of nanoparticles per plasmid DNA was estimated to be 54. The magnetic relaxivity of these DNA-bound NPs, determined by measuring the relaxation time as a function of the nanoparticle concentration using MRI, was ~279 s^{-1} mM^{-1}.

MRI of Glioma Tumor Xenografts. To evaluate the ability of the developed nanovector to penetrate throughout the tumor, control and targeting nanovectors (NP:DNA and NP:DNA−CTX, respectively) were administered systemically through the tail vein to mice bearing C6 xenograft flank tumors. Nanovector accumulation in the tumor was monitored using MRI 48 h post-treatment (Figure 3a). The R_2 maps show that there was an increase in R_2 postinjection in both NP:DNA and NP: DNA−CTX treated mice, which indicates nanovector accumulation in the tumor site. However, there was no difference between the contrast enhancements provided by NP:DNA and NP:DNA−CTX, which is quantitatively shown in Figure 3b. Figure 3c shows that there was no contrast enhancement in the muscle, which indicates these nanovectors extravasate from the blood vessel into the tumor site through the EPR effect. Since the sizes and ζ potentials of NP:DNA and NP:DNA−CTX were similar, there was no difference in this passive tumor targeting through the EPR effect.

***Ex Vivo* Optical Imaging of Delivered Gene Expression.** To assess *in vivo* gene delivery through administration of nanovectors, tumors and relevant clearance organs were evaluated for GFP expression using optical fluorescence imaging. Mice with C6 xenograft tumors were treated, as described above, and sacrificed 48 h post-treatment. Tumors and clearance organs were resected and imaged for GFP fluorescence using a Xenogen IVIS imaging system (Figure 4a). Tumors from mice treated with the targeted nanovector, NP:DNA−CTX, had a much higher fluorescence intensity than those from mice treated with the nontargeted nanovector, NP:
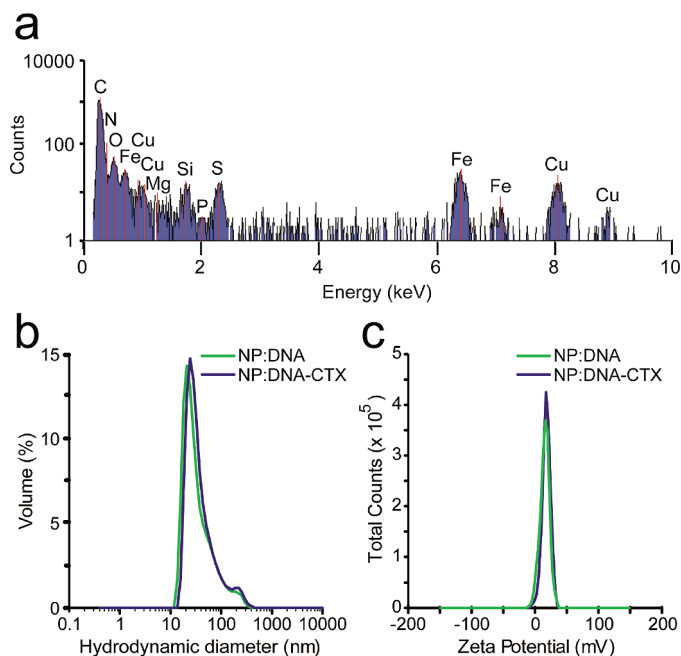

Figure 2. Physicochemical characterization of nanovectors. (a) Energy dispersive X-ray (EDX) spectrum of NP:DNA confirming the presence of the iron oxide nanoparticle core (Fe peaks), polymer coating (C, N, O, and S peaks), and DNA (C and P peaks). The copper peaks come from the TEM grid. (b) Size distribution of NP:DNA and NP:DNA−CTX as determined by dynamic light scattering. (c) The ζ potential distribution of NP: DNA and NP:DNA−CTX as determined by dynamic light scattering.

DNA, whereas the livers, kidneys, and spleens all showed similar fluorescence intensities regardless of nanovector treatment. Furthermore, the GFP expression was more uniformly distributed throughout the tumor from NP:DNA−CTX treated mice, whereas expression was found in more localized regions in the tumors from NP:DNA treated mice. GFP fluorescence quantification (Figure 4b) in the tumors from NP:DNA treated mice (1195 ± 117 counts) and NP:DNA−CTX treated mice (1840 ± 375 counts) showed that there was a marked increase in GFP fluorescence as a result of CTX targeting ($P < 0.05$, $n = 3$). There were no statistical differences in the GFP fluorescence quantifications from the livers, kidneys, and spleens, which shows off-target uptake and expression was not affected by CTX targeting. This reveals the tumor cell specificity of this targeting molecule since the enhanced expression was only observed in target cells. These data indicate that the targeting ability of CTX functions through enhancing uptake into a higher proportion of target cells. Off-target expression in the liver and kidney could cause deleterious effects upon delivery of a therapeutic gene, and it is clear the targeting ligand does not reduce the off-target uptake and expression of the delivered gene. To circumvent this problem, the delivered therapeutic gene should be designed to ensure that the expression of delivered genes would be limited to only the target cells. This has been achieved by using tumor-specific promoters that are not present in off-target cells.[40,41]
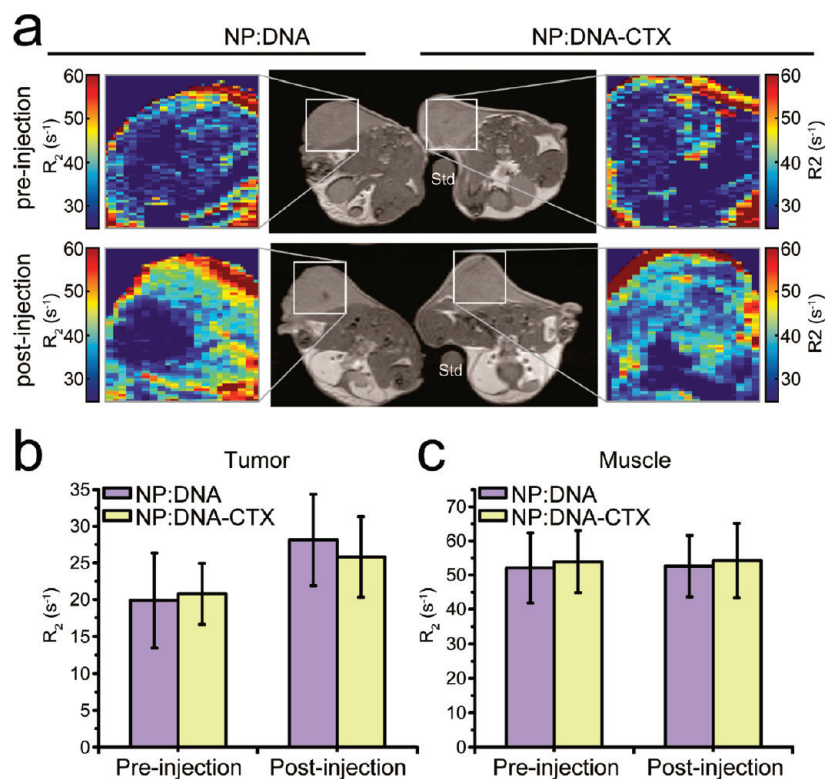
Figure 3. Nanovector delivery to C6 xenograft tumors monitored by MRI. a) T_2-weighted images of C6 xenograft tumor bearing mice with an agarose mold standard (Std) and with colorized R_2 expanded views of the tumor regions for both NP: DNA (left) and NP:DNA−CTX (right) treatments. Both nontargeted (NP:DNA) and targeted (NP:DNA−CTX) nanovector treated tumors showed similar enhancement of R_2 contrast. **(b)** Quantitative R_2 values for the tumor region in NP:DNA and NP: DNA−CTX treated mice. **(c)** Quantitative R_2 values for muscle in NP:DNA and NP:DNA−CTX treated mice.

The CTX-mediated targeting was further confirmed by histological and confocal analyses of resected tu-
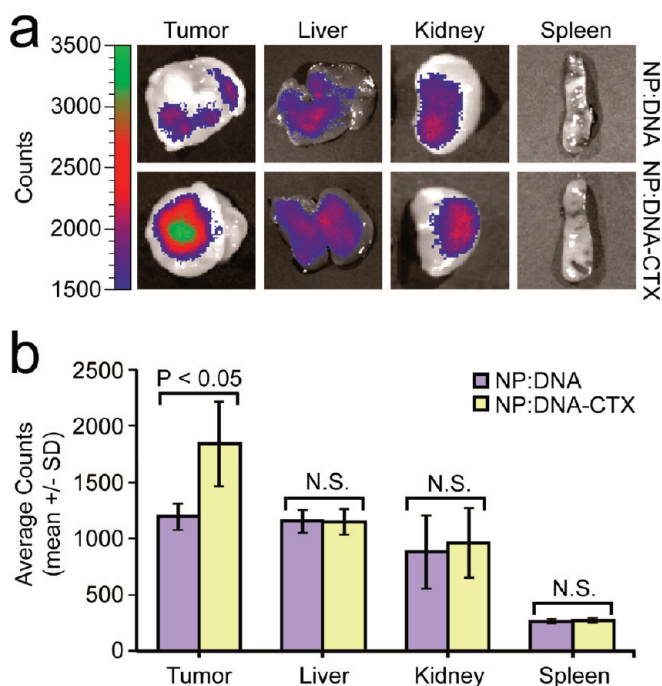

Figure 4. Enhanced delivery of GFP encoding DNA to C6 glioma cells *in vivo* using chlorotoxin labeled NPs. (a) Xenogen images of tumors, livers, kidneys, and spleens from C6 xenograft tumor bearing mice, harvested 48 h after treatment, indicating GFP fluorescence levels. **(b)** Average counts over the tumors and clearance organs, quantified using the IVIS Xenogen software ($n = 3$).

mors (Figures 5 and 6). Prussian blue staining of iron showed that the amount of nanovector accumulation in the tumor site was similar for both nontargeted (NP: DNA) and targeted (NP:DNA−CTX) nanovectors (Figure 5a), consistent with the MR images. Nontargeted NP: DNA accumulation occurred in more localized regions, whereas targeted NP:DNA−CTX accumulation was much more distributed throughout the tumor. Furthermore, tumor sections imaged at higher magnification revealed that the NP:DNA−CTX had higher intracellular localization compared to that of NP:DNA (Figure 5b). This shows a definite difference in behavior of the nanovectors once they extravasate from the blood vessel into the tumor site, specifically due to the CTX. The localized accumulations of nontargeted nanovectors were probably the result of minimal cell uptake and trafficking. On the other hand, the CTX targeted nanovectors were readily taken up by target cells due to specific interaction with the receptor on the cell membrane and distributed around the tumor, similar to previous results using CTX targeted nanoparticles.[18] This allowed for a higher proportion of cells to be exposed to the gene delivery vehicle for transfection. Other studies using targeted nanoparticles have observed similar results that nanoparticle accumulation in tumors is not increased by the addition of a targeting ligand but uptake of the nanoparticles by target cells is enhanced.[42−45] Recent studies have found that
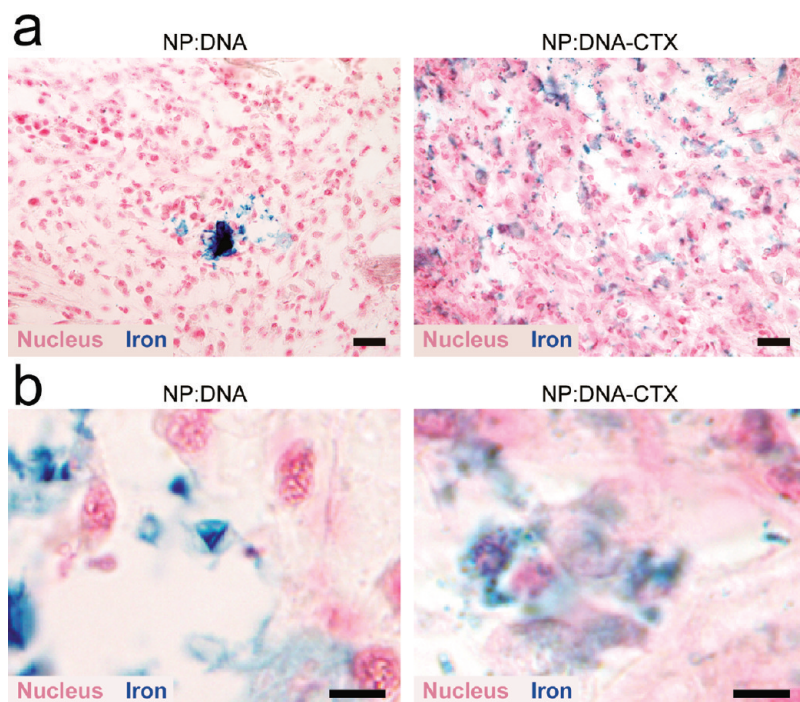
Figure 5. Histology analysis of C6 xenograft tumors showing NP distribution. (a) Prussian blue stained sections of tumors from mice treated with nontargeted (NP:DNA) and targeted (NP:DNA−CTX) nanovectors. Scale bar corresponds to 20 μm. (b) Images of Prussian blue stained sections at high magnification for better visualization of nanovector localization. Scale bar corresponds to 5 μm.

PEGylated nanoparticles accumulate in tumors *via* the EPR effect regardless of the presence of a targeting agent.[38] Here, the gene delivery vehicle must interact with the cell membrane to promote uptake into the cell. Most of the cationic nonviral vectors studied are nonspecifically taken up by cells through absorptive-mediated endocytosis. This nonspecific targeting is inefficient since the positively charged vehicle would not only interact with the negatively charged cell membrane but also with the negatively charged extracellular matrix proteins present in the tumor microenvironment. The addition of a targeting agent allows the delivery vehicle to interact specifically with the cancer cells through the high-affinity binding of targeting ligand to cell surface receptor.

To confirm that higher exposure of cells to the gene delivery vehicle is responsible for the elevated expression of the delivered gene at the cellular level, confocal fluorescence microscopy was performed on tumor sections from NP:DNA and NP:DNA−CTX nanovector treated mice 48 h post-treatment (Figure 6). More cells expressing GFP were visible in tumors treated with the targeted nanovectors (NP:DNA−CTX) as expected, which shows that CTX plays a critical role in promoting nanovector uptake by target cells and greatly enhances the transfection efficiency of NP:DNA−CTX specifically in target cells. Exposing a higher number of cells to a delivered therapeutic should greatly improve the efficacy of the therapy.

CONCLUSIONS

Here we report on the use of chlorotoxin (CTX) targeted nanoparticles loaded with DNA to enhance uptake specifically into glioma cells *in vivo*. Importantly, by
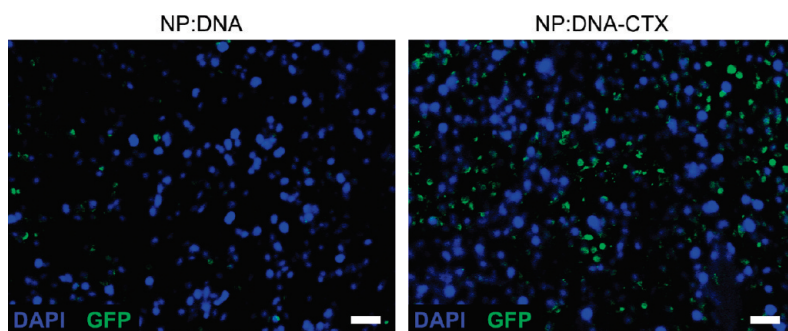

Figure 6. Confocal fluorescence images of tumor sections from NP:DNA and NP:DNA−CTX treated mice. Specific uptake of NP:DNA−CTX dramatically enhanced the transfection efficiency causing a larger number of cells in tumors to express GFP. Scale bars correspond to 20 μm.

using a vehicle that could be monitored *in situ*, we found that nanovector uptake into the cancer cells in the tumor site was enhanced specifically due to CTX, as evidenced by the increase in GFP expression, and that biodistribution and accumulation in the tumor site was not affected by the targeting ligand. While CTX does not enhance DNA loaded nanovector accumulation in the xenograft tumor site, it does promote specific uptake of nanovectors into glioma cells, exposing a higher proportion of target cells to the delivered payload. These results could provide insight into the design of more effective gene delivery vehicles for improved treatment outcome of gene therapy for glioma and other deadly cancers.

METHODS

Materials. Polyethylenimine (PEI; average MW = 1.2 kDa), chitosan (medium molecular weight), methoxy poly(ethylene glycol) (mPEG; MW = 2 kDa), and other reagents were purchased from Sigma-Aldrich (St. Louis, MO) unless otherwise specified.

Plasmid DNA Preparation. Enhanced green fluorescent protein (EGFP) encoding DNA under control of the cytomegalovirus (CMV) promoter in the CS2 vector (pEGFP-CS2) was propagated in DH5-α *E. coli* and purified using the Plasmid Giga Kit (Qiagen, Valencia, CA). Purified pEGFP-CS2, with an A_{260}/A_{280} purity between 1.8 and 1.9, was dissolved in TE buffer at 1 mg/mL and stored at -20 °C.

Nanovector Synthesis. Base nanoparticles were prepared, as reported previously,[18,32] and outlined in Figure 1. NP-CP-PEI (herein called NP) were complexed with pEGFP-CS2 at a weight ratio of 10:1 (Fe equivalent of NP:DNA) in reaction buffer (20 mM of HEPES, 5 mM of EDTA, and pH = 7.2) for 30 min. Chlorotoxin (CTX, Alamone Laboratories, Jerusalem, Israel) was conjugated to DNA-loaded NPs using a heterobifunctional PEG linker. Then 250 μg of CTX was dissolved in 125 μL of reaction buffer, and 4.05 μL of a 5 mg/mL solution of 2-iminothiolane (Traut's reagent, Molecular Biosciences, Boulder, CO) was added and allowed to react for 1 h to form CTX$-$Traut's. An identical solution without CTX was also prepared. One μL of a 250 mM solution of NHS-PEG$_{12}$$-$maleimide (Thermo Fisher Scientific, Rockford, IL) was added to 1 mL of DNA-loaded NPs in reaction buffer (1 mg of Fe/mL) and allowed to react for 30 min. Unreacted PEG was washed away from NPs using a PD-10 desalting column (GE Healthcare, Piscataway, NJ) equilibrated with reaction buffer. NPs were then mixed with the CTX$-$Traut's and allowed to react for 30 min before washing away unreacted CTX using S-200 sephacryl resin equilibrated with 20 mM of HEPES buffer (pH 7.4) to form NP:DNA$-$CTX. NPs were also mixed with the Traut's solution without CTX to form NP:DNA as a control. To quantify the amount of CTX on the NP, sodium dodecyl sulfate polyacrylamide gel electrophoresis (SDS-PAGE) was run on the unpurified NP:DNA$-$CTX reaction solution, stained with Bio-Safe Coomassie Blue (Bio-Rad, Hercules, CA), and imaged using a ChemiDoc XRS system (Bio-Rad, Hercules, CA). Unbound CTX was quantified using the Quantity One software package (Bio-Rad, Hercules, CA) based on a standard curve and subtracted from the total amount of CTX in the reaction to obtain the amount of CTX on the NP.

In Vivo Studies. All animal experiments were conducted in accordance with University of Washington Institutional Animal Care and Use Committee (IACUC) approved protocols. Flank xenograft tumors of C6 cells were prepared by subcutaneous injection of one million cells suspended in serum free media and Matrigel (BD Biosciences, San Jose, CA) into male nu/nu mice (Charles River, Wilmington, MA). Tumors were allowed to grow for 4 weeks before mice were injected intravenously through the tail vein with 200 μL of NP:DNA or NP-DNA$-$CTX complex (0.7 mg Fe/ml) for a final dose of 14 μg of pEGFP-CS2 per animal. Then 48 h after treatment, tumors, livers, kidneys, and spleens were excised and imaged using a Xenogen IVIS-100 system (Caliper Life Sciences, Hopkinton, MA). The timing of 48 h was found to be the appropriate time for the nanoparticles to circulate in the bloodstream and accumulate in the tumor for our mouse model based on our previous studies.[18,31]

Magnetic Resonance Imaging. MR images were obtained before and 48 h after treatment with the NP:DNA or NP-DNA$-$CTX complex on a 4.7T Bruker magnet (Bruker Medical Systems, Karlsruhe, Germany) equipped with Varian Inova spectrometer (Varian, Inc., Palo Alto, CA). Mice were anesthetized with $1-2.5\%$ isofluorane (Abbott Laboratories, Abbott Park, IL) before they were placed in the imaging chamber. A 6 cm inner diameter quadrature volume coil and spin$-$echo imaging sequence were used to acquire T_2-weighted images. A spin$-$echo multislice imaging sequence was used to determine T_2 values in tumor tissues using the following imaging parameters: TR = 2 s, TE = 13.4, 30, and 60 ms, field of view = 60×30 mm^2, number of averages = 2, matrix size = 256×128, slice number = 10, slice thickness = 1 mm, and slice gap = 0.5 mm. The T_2 map was generated by NIH ImageJ (Bethesda, MD) based on the equation, SI = $A*\exp(-TE/T2) + B$, where SI is the signal intensity, TE is the echo time, A is the amplitude, and B is the offset. The R_2 map was generated by taking the reciprocal of the T_2 map.

Histological and Confocal Analyses. Excised organs were placed into 30% sucrose in phosphate buffered saline (PBS), embedded in optimal cutting temperature (OCT) compound, and stored at -80 °C. Eight μm frozen sections were stained with Prussian blue and nucleus fast red according to standard histopathology protocols. Images were obtained on an Eclipse E600 upright microscope (Nikon Instruments, Melville, NY). For confocal analysis, 8 μm frozen tumor sections were washed with PBS, fixed, and permeabilized with ice-cold acetone, and stained with anti-GFP primary and FITC-labeled secondary antibodies (Abcam, Cambridge, MA), following the manufacturer's protocol. Stained sections were then mounted in Prolong Gold antifade solution (Invitrogen, Carlsbad, CA) containing DAPI for cell nuclei staining and imaged on an LSM 510 meta confocal fluorescence microscope (Carl Zeiss Inc., Peabody, MA) with the appropriate filters.

REFERENCES AND NOTES

1. Germano, I. M.; Binello, E. Gene Therapy as an Adjuvant Treatment for Malignant Gliomas: From Bench to Bedside. *J. Neuro-Oncol.* **2009**, *93*, 79–87.
2. Williams, D. A. Rac Reviews Serious Adverse Event Associated with Aav Therapy Trial. *Mol. Ther.* **2007**, *15*, 2053–2054.
3. Zhang, X.; Godbey, W. T. Viral Vectors for Gene Delivery in Tissue Engineering. *Adv. Drug Delivery Rev.* **2006**, *58*, 515–534.
4. Mintzer, M. A.; Simanek, E. E. Nonviral Vectors for Gene Delivery. *Chem. Rev.* **2009**, *109*, 259–302.
5. Scherer, F.; Anton, M.; Schillinger, U.; Henke, J.; Bergemann, C.; Kruger, A.; Gansbacher, B.; Plank, C. Magnetofection: Enhancing and Targeting Gene Delivery by Magnetic Force *in Vitro* and *in Vivo*. *Gene Ther.* **2002**, *9*, 102–109.
6. Namiki, Y.; Namiki, T.; Yoshida, H.; Ishii, Y.; Tsubota, A.; Koido, S.; Nariai, K.; Mitsunaga, M.; Yanagisawa, S.;

Kashiwagi, H.; et al. A Novel Magnetic Crystal-Lipid Nanostructure for Magnetically Guided *in Vivo* Gene Delivery. *Nat. Nanotechnol.* **2009**, *4*, 598–606.

7. Mirimanoff, R. O.; Gorlia, T.; Mason, W.; Van den Bent, M. J.; Kortmann, R. D.; Fisher, B.; Reni, M.; Brandes, A. A.; Curschmann, J.; Villa, S.; et al. Radiotherapy and Temozolomide for Newly Diagnosed Glioblastoma: Recursive Partitioning Analysis of the Eortc 26981/22981-Ncic Ce3 Phase Iii Randomized Trial. *J. Clin. Oncol.* **2006**, *24*, 2563–2569.

8. Stupp, R.; Mason, W. P.; van den Bent, M. J.; Weller, M.; Fisher, B.; Taphoorn, M. J.; Belanger, K.; Brandes, A. A.; Marosi, C.; Bogdahn, U.; et al. Radiotherapy Plus Concomitant and Adjuvant Temozolomide for Glioblastoma. *N. Engl. J. Med.* **2005**, *352*, 987–996.

9. Vredenburgh, J. J.; Desjardins, A.; Herndon, J. E., II; Dowell, J. M.; Reardon, D. A.; Quinn, J. A.; Rich, J. N.; Sathornsumetee, S.; Gururangan, S.; Wagner, M.; et al. Phase Ii Trial of Bevacizumab and Irinotecan in Recurrent Malignant Glioma. *Clin. Cancer Res.* **2007**, *13*, 1253–1259.

10. Ogris, M.; Walker, G.; Blessing, T.; Kircheis, R.; Wolschek, M.; Wagner, E. Tumor-Targeted Gene Therapy: Strategies for the Preparation of Ligand-Polyethylene Glycol-Polyethylenimine/DNA Complexes. *J. Controlled Release* **2003**, *91*, 173–181.

11. Kircheis, R.; Schuller, S.; Brunner, S.; Ogris, M.; Heider, K. H.; Zauner, W.; Wagner, E. Polycation-Based DNA Complexes for Tumor-Targeted Gene Delivery *in Vivo*. *J. Gene Med.* **1999**, *1*, 111–120.

12. Jiang, H. L.; Kwon, J. T.; Kim, E. M.; Kim, Y. K.; Arote, R.; Jere, D.; Jeong, H. J.; Jang, M. K.; Nah, J. W.; Xu, C. X.; et al. Galactosylated Poly(Ethylene Glycol)-Chitosan-Graft-Polyethylenimine as a Gene Carrier for Hepatocyte-Targeting. *J. Controlled Release* **2008**, *131*, 150–157.

13. Wolschek, M. F.; Thallinger, C.; Kursa, M.; Rossler, V.; Allen, M.; Lichtenberger, C.; Kircheis, R.; Lucas, T.; Willheim, M.; Reinisch, W.; et al. Specific Systemic Nonviral Gene Delivery to Human Hepatocellular Carcinoma Xenografts in Scid Mice. *Hepatology* **2002**, *36*, 1106–1114.

14. Huang, H.; Yu, H.; Tang, G.; Wang, Q.; Li, J. Low Molecular Weight Polyethylenimine Cross-Linked by 2-Hydroxypropyl-Gamma-Cyclodextrin Coupled to Peptide Targeting Her2 as a Gene Delivery Vector. *Biomaterials* **2010**, *31*, 1830–1838.

15. Moffatt, S.; Papasakelariou, C.; Wiehle, S.; Cristiano, R. Successful *in Vivo* Tumor Targeting of Prostate-Specific Membrane Antigen with a Highly Efficient J591/Pei/DNA Molecular Conjugate. *Gene Ther.* **2006**, *13*, 761–772.

16. Xu, L.; Huang, C. C.; Huang, W.; Tang, W. H.; Rait, A.; Yin, Y. Z.; Cruz, I.; Xiang, L. M.; Pirollo, K. F.; Chang, E. H. Systemic Tumor-Targeted Gene Delivery by Anti-Transferrin Receptor Scfv-Immunoliposomes. *Mol. Cancer Ther.* **2002**, *1*, 337–346.

17. Yang, Y.; Zhang, Z.; Chen, L.; Gu, W.; Li, Y. Galactosylated Poly(2-(2-Aminoethyoxy)Ethoxy)Phosphazene/DNA Complex Nanoparticles: In Vitro and in Vivo Evaluation for Gene Delivery. *Biomacromolecules* **2010**, *11*, 927–933.

18. Veiseh, O.; Sun, C.; Fang, C.; Bhattarai, N.; Gunn, J.; Kievit, F.; Du, K.; Pullar, B.; Lee, D.; Ellenbogen, R. G.; et al. Specific Targeting of Brain Tumors with an Optical/Magnetic Resonance Imaging Nanoprobe across the Blood-Brain Barrier. *Cancer Res.* **2009**, *69*, 6200–6207.

19. Tsutsui, Y.; Tomizawa, K.; Nagita, M.; Michiue, H.; Nishiki, T.; Ohmori, I.; Seno, M.; Matsui, H. Development of Bionanocapsules Targeting Brain Tumors. *J. Controlled Release* **2007**, *122*, 159–164.

20. Ying, X.; Wen, H.; Lu, W. L.; Du, J.; Guo, J.; Tian, W.; Men, Y.; Zhang, Y.; Li, R. J.; Yang, T. Y.; et al. Dual-Targeting Daunorubicin Liposomes Improve the Therapeutic Efficacy of Brain Glioma in Animals. *J. Controlled Release* **2010**, *141*, 183–192.

21. Reddy, G. R.; Bhojani, M. S.; McConville, P.; Moody, J.; Moffat, B. A.; Hall, D. E.; Kim, G.; Koo, Y. E.; Woolliscroft, M. J.; Sugai, J. V.; et al. Vascular Targeted Nanoparticles for Imaging and Treatment of Brain Tumors. *Clin. Cancer Res.* **2006**, *12*, 6677–6686.

22. Koo, Y. E.; Reddy, G. R.; Bhojani, M.; Schneider, R.; Philbert, M. A.; Rehemtulla, A.; Ross, B. D.; Kopelman, R. Brain Cancer Diagnosis and Therapy with Nanoplatforms. *Adv. Drug Delivery Rev.* **2006**, *58*, 1556–1577.

23. Zhang, Y.; Jeong Lee, H.; Boado, R. J.; Pardridge, W. M. Receptor-Mediated Delivery of an Antisense Gene to Human Brain Cancer Cells. *J. Gene Med.* **2002**, *4*, 183–194.

24. Lu, W.; Sun, Q.; Wan, J.; She, Z.; Jiang, X. G. Cationic Albumin-Conjugated Pegylated Nanoparticles Allow Gene Delivery into Brain Tumors *Via* Intravenous Administration. *Cancer Res.* **2006**, *66*, 11878–11887.

25. Kohler, N.; Sun, C.; Fichtenholtz, A.; Gunn, J.; Fang, C.; Zhang, M. Methotrexate-Immobilized Poly(Ethylene Glycol) Magnetic Nanoparticles for Mr Imaging and Drug Delivery. *Small* **2006**, *2*, 785–792.

26. Lyons, S. A.; O'Neal, J.; Sontheimer, H. Chlorotoxin, a Scorpion-Derived Peptide, Specifically Binds to Gliomas and Tumors of Neuroectodermal Origin. *Glia* **2002**, *39*, 162–173.

27. Veiseh, M.; Gabikian, P.; Bahrami, S. B.; Veiseh, O.; Zhang, M.; Hackman, R. C.; Ravanpay, A. C.; Stroud, M. R.; Kusuma, Y.; Hansen, S. J.; et al. Tumor Paint: A Chlorotoxin:Cy5.5 Bioconjugate for Intraoperative Visualization of Cancer Foci. *Cancer Res.* **2007**, *67*, 6882–6888.

28. Sun, C.; Veiseh, O.; Gunn, J.; Fang, C.; Hansen, S.; Lee, D.; Sze, R.; Ellenbogen, R. G.; Olson, J.; Zhang, M. In Vivo MRI Detection of Gliomas by Chlorotoxin-Conjugated Superparamagnetic Nanoprobes. *Small* **2008**, *4*, 372–379.

29. Sun, C.; Fang, C.; Stephen, Z.; Veiseh, O.; Hansen, S.; Lee, D.; Ellenbogen, R. G.; Olson, J.; Zhang, M. Q. Tumor-Targeted Drug Delivery and MRI Contrast Enhancement by Chlorotoxin-Conjugated Iron Oxide Nanoparticles. *Nanomedicine* **2008**, *3*, 495–505.

30. Veiseh, O.; Sun, C.; Gunn, J.; Kohler, N.; Gabikian, P.; Lee, D.; Bhattarai, N.; Ellenbogen, R.; Sze, R.; Hallahan, A.; et al. Optical and MRI Multifunctional Nanoprobe for Targeting Gliomas. *Nano Lett.* **2005**, *5*, 1003–1008.

31. Sun, C.; Du, K.; Fang, C.; Bhattarai, N.; Veiseh, O.; Kievit, F.; Stephen, Z.; Lee, D.; Ellenbogen, R. G.; Ratner, B.; et al. Peg-Mediated Synthesis of Highly Dispersive Multifunctional Superparamagnetic Nanoparticles: Their Physicochemical Properties and Function *in Vivo*. *ACS Nano* **2010**, *4*, 2402–2410.

32. Kievit, F. M.; Veiseh, O.; Bhattarai, N.; Fang, C.; Gunn, J. W.; Lee, D.; Ellenbogen, R. G.; Olson, J. M.; Zhang, M. Pei-Peg-Chitosan Copolymer Coated Iron Oxide Nanoparticles for Safe Gene Delivery: Synthesis, Complexation, and Transfection. *Adv. Funct. Mater.* **2009**, *19*, 2244–2251.

33. Lee, J.; Veiseh, O.; Bhattarai, N.; Sun, C.; Hansen, S. J.; Ditzler, S.; Knoblaugh, S.; Lee, D.; Ellenbogen, R.; Zhang, M.; et al. Rapid Pharmacokinetic and Biodistribution Studies Using Cholorotoxin-Conjugated Iron Oxide Nanoparticles: A Novel Non-Radioactive Method. *PLoS One* , *5*, e9536.

34. Boussif, O.; Lezoualc'h, F.; Zanta, M. A.; Mergny, M. D.; Scherman, D.; Demeneix, B.; Behr, J. P. A Versatile Vector for Gene and Oligonucleotide Transfer into Cells in Culture and *in Vivo*: Polyethylenimine. *Proc. Natl. Acad. Sci. U.S.A.* **1995**, *92*, 7297–7301.

35. Kondo, T.; Setoguchi, T.; Taga, T. Persistence of a Small Subpopulation of Cancer Stem-Like Cells in the C6 Glioma Cell Line. *Proc. Natl. Acad. Sci. U.S.A.* **2004**, *101*, 781–786.

36. Alexis, F.; Pridgen, E.; Molnar, L. K.; Farokhzad, O. C. Factors Affecting the Clearance and Biodistribution of Polymeric Nanoparticles. *Mol. Pharm.* **2008**, *5*, 505–515.

37. Longmire, M.; Choyke, P. L.; Kobayashi, H. Clearance Properties of Nano-Sized Particles and Molecules as Imaging Agents: Considerations and Caveats. *Nanomedicine* **2008**, *3*, 703–717.

38. Pirollo, K. F.; Chang, E. H. Does a Targeting Ligand Influence Nanoparticle Tumor Localization or Uptake. *Trends Biotechnol.* **2008**, *26*, 552–558.

39. Veiseh, O.; Gunn, J. W.; Zhang, M. Design and Fabrication of Magnetic Nanoparticles for Targeted Drug Delivery and Imaging. *Adv. Drug Delivery Rev.* **2010**, *62*, 284–304.

40. Zhang, Y.; Wang, C. W.; Wang, Z. G.; Ma, D. X.; Pan, S.; Zhu, S. G.; Li, F.; Wang, B. Construction of Double Suicide Genes System Controlled by Mdr1 Promoter with Targeted Expression in Drug-Resistant Glioma Cells. *J. Neuro-Oncol.* **2008**, *86*, 3–11.

41. Boulaire, J.; Balani, P.; Wang, S. Transcriptional Targeting to Brain Cells: Engineering Cell Type-Specific Promoter Containing Cassettes for Enhanced Transgene Expression. *Adv. Drug Delivery Rev.* **2009**, *61*, 589–602.

42. Kirpotin, D. B.; Drummond, D. C.; Shao, Y.; Shalaby, M. R.; Hong, K.; Nielsen, U. B.; Marks, J. D.; Benz, C. C.; Park, J. W. Antibody Targeting of Long-Circulating Lipidic Nanoparticles Does Not Increase Tumor Localization but Does Increase Internalization in Animal Models. *Cancer Res.* **2006**, *66*, 6732–6740.

43. Bartlett, D. W.; Su, H.; Hildebrandt, I. J.; Weber, W. A.; Davis, M. E. Impact of Tumor-Specific Targeting on the Biodistribution and Efficacy of Sirna Nanoparticles Measured by Multimodality *in Vivo* Imaging. *Proc. Natl. Acad. Sci. U.S.A.* **2007**, *104*, 15549–15554.

44. Choi, C. H.; Alabi, C. A.; Webster, P.; Davis, M. E. Mechanism of Active Targeting in Solid Tumors with Transferrin-Containing Gold Nanoparticles. *Proc. Natl. Acad. Sci. U.S.A.* **2010**, *107*, 1235–1240.

45. Wang, X.; Li, J.; Wang, Y.; Cho, K. J.; Kim, G.; Gjyrezi, A.; Koenig, L.; Giannakakou, P.; Shin, H. J.; Tighiouart, M.; et al. Hft-T, a Targeting Nanoparticle, Enhances Specific Delivery of Paclitaxel to Folate Receptor-Positive Tumors. *ACS Nano* **2009**, *3*, 3165–3174.